

## PROOF COVER SHEET

---

Author(s): B. Montgomery Pettitt

Article title: Accelerating the weighted histogram analysis method by direct inversion in the iterative subspace

Article no: GMOS 1110583

Enclosures: 1) Query sheet  
2) Article proofs

---

Dear Author,

Please find attached the proofs for your article.

**1. Please check these proofs carefully.** It is the responsibility of the corresponding author to check these and approve or amend them. A second proof is not normally provided. Taylor & Francis cannot be held responsible for uncorrected errors, even if introduced during the production process. Once your corrections have been added to the article, it will be considered ready for publication

Please limit changes at this stage to the correction of errors. You should not make trivial changes, improve prose style, add new material, or delete existing material at this stage. You may be charged if your corrections are excessive (we would not expect corrections to exceed 30 changes).

For detailed guidance on how to check your proofs, please paste this address into a new browser window: <http://journalauthors.tandf.co.uk/production/checkingproofs.asp>


Your PDF proof file has been enabled so that you can comment on the proof directly using Adobe Acrobat. If you wish to do this, please save the file to your hard disk first. For further information on marking corrections using Acrobat, please paste this address into a new browser window: <http://journalauthors.tandf.co.uk/production/acrobat.asp>

---

**2. Please review the table of contributors below and confirm that the first and last names are structured correctly and that the authors are listed in the correct order of contribution.** This check is to ensure that your names will appear correctly online and when the article is indexed.

Sequence	Prefix	Given name(s)	Surname	Suffix
1		Cheng	Zhang	
2		Chun-Liang	Lai	
3		B. Montgomery	Pettitt	

Queries are marked in the margins of the proofs, and you can also click the hyperlinks below.

Content changes made during copy-editing are shown as tracked changes. Inserted text is in **red font** and revisions have a **blue** indicator . Changes can also be viewed using the list comments function. To correct the proofs, you should insert or delete text following the instructions below, but **do not add comments to the existing tracked changes**.

## AUTHOR QUERIES

### General points:

1. **Permissions:** You have warranted that you have secured the necessary written permission from the appropriate copyright owner for the reproduction of any text, illustration, or other material in your article. For further guidance on this topic please see: <http://journalauthors.tandf.co.uk/copyright/usingThirdPartyMaterial.asp>
2. **Third-party material:** If there is material in your article that is owned by a third party, please check that the necessary details of the copy-right/rights owner are shown correctly.
3. **Affiliation:** The corresponding author is responsible for ensuring that address and email details are correct for all the co-authors. Affiliations given in the article should be the affiliation at the time the research was conducted. For further guidance on this topic please see: <http://journalauthors.tandf.co.uk/preparation/writing.asp>.
4. **Funding:** Was your research for this article funded by a funding agency? If so, please insert 'This work was supported by <insert the name of the funding agency in full>', followed by the grant number in square brackets '[grant number xxxx]'.
5. **Supplemental data and underlying research materials:** Do you wish to include the location of the underlying research materials (e.g. data, samples or models) for your article? If so, please insert this sentence before the reference section: 'The underlying research materials for this article can be accessed at <full link>/ description of location [author to complete]'. If your article includes supplemental data, the link will also be provided in this paragraph. See <http://journalauthors.tandf.co.uk/preparation/multimedia.asp> for further explanation of supplemental data and underlying research materials.
6. The **CrossRef database** ([www.crossref.org/](http://www.crossref.org/)) has been used to validate the references. Changes resulting from mismatches are tracked in **red** font.

AQ1	Please check whether the e-mail address has been set correctly.
AQ2	The disclosure statement has been inserted. Please correct if this is inaccurate.
AQ3	Please provide missing publisher location for the Ref. [5].
AQ4	Please provide missing chapter title, editor name and last page for the Ref. [23].
AQ5	Please provide missing publisher location for the Ref. [49]
AQ6	Please provide missing editor name, publisher location and page numbers for the Ref. [50].
AQ7	Please provide missing publisher location for the Ref [51].
AQ8	Please provide missing publisher location for the Ref. [52].
AQ9	Please provide missing publisher location for Ref. [64].
AQ10	Please provide missing editor name and publisher location for the Ref. [70].
AQ11	Please provide missing publisher location for the Ref. [71].
AQ12	Please provide missing publisher location for the Ref. [73].

## How to make corrections to your proofs using Adobe Acrobat/Reader

Taylor & Francis offers you a choice of options to help you make corrections to your proofs. Your PDF proof file has been enabled so that you can mark up the proof directly using Adobe Acrobat/Reader. This is the simplest and best way for you to ensure that your corrections will be incorporated. If you wish to do this, please follow these instructions:

1. Save the file to your hard disk.
2. Check which version of Adobe Acrobat/Reader you have on your computer. You can do this by clicking on the “Help” tab, and then “About”.

If Adobe Reader is not installed, you can get the latest version free from <http://get.adobe.com/reader/>.

3. If you have Adobe Acrobat/Reader 10 or a later version, click on the “Comment” link at the right-hand side to view the Comments pane.
4. You can then select any text and mark it up for deletion or replacement, or insert new text as needed. Please note that these will clearly be displayed in the Comments pane and secondary annotation is not needed to draw attention to your corrections. If you need to include new sections of text, it is also possible to add a comment to the proofs. To do this, use the Sticky Note tool in the task bar. Please also see our FAQs here: <http://journalauthors.tandf.co.uk/production/index.asp>.
5. Make sure that you save the file when you close the document before uploading it to CATS using the “Upload File” button on the online correction form. If you have more than one file, please zip them together and then upload the zip file.

If you prefer, you can make your corrections using the CATS online correction form.

## Troubleshooting

**Acrobat help:**<http://helpx.adobe.com/acrobat.html>

**Reader help:**<http://helpx.adobe.com/reader.html>

Please note that full user guides for earlier versions of these programs are available from the Adobe Help pages by clicking on the link “Previous versions” under the “Help and tutorials” heading from the relevant link above. Commenting functionality is available from Adobe Reader 8.0 onwards and from Adobe Acrobat 7.0 onwards.

**Firefox users:** Firefox’s inbuilt PDF Viewer is set to the default; please see the following for instructions on how to use this and download the PDF to your hard drive:

[http://support.mozilla.org/en-US/kb/view-pdf-files-firefox-without-downloading-them#w\\_using-a-pdf-reader-plugin](http://support.mozilla.org/en-US/kb/view-pdf-files-firefox-without-downloading-them#w_using-a-pdf-reader-plugin)

# Accelerating the weighted histogram analysis method by direct inversion in the iterative subspace

Cheng Zhang, Chun-Liang Lai and B. Montgomery Pettitt

Sealy Center for Structural Biology and Molecular Biophysics, The University of Texas Medical Branch, Galveston, TX, USA

5



## ABSTRACT

The weighted histogram analysis method (WHAM) for free energy calculations is a valuable tool to produce free energy differences with the minimal errors. Given multiple simulations, WHAM obtains from the distribution overlaps the optimal statistical estimator of the density of states, from which the free energy differences can be computed. The WHAM equations are often solved by an iterative procedure. In this work, we use a well-known linear algebra algorithm which allows for more rapid convergence to the solution. We find that the computational complexity of the iterative solution to WHAM, and the closely-related multiple Bennett acceptance ratio method can be improved using the method of direct inversion in the iterative subspace. We give examples from a lattice model, a simple liquid and an aqueous protein solution.

## ARTICLE HISTORY

Received 7 August 2015  
Accepted 14 October 2015

## KEYWORDS

Free energy; WHAM; MBAR; DIIS

## 1. Introduction

An important problem in computational physics and chemistry is to obtain the best estimate of a quantity of interest from a given set of data.[1] For free energy calculations, the multiple histogram method [2–5] or its generalisation, the weighted histogram analysis method (WHAM),[1,6–17] is an effective tool for addressing such a problem. WHAM is statistically efficient in using the data acquired from molecular simulations, and it has become a standard free energy analysis tool, particularly popular for enhanced-sampling simulations, such as umbrella sampling,[18,19] and simulated [20,21] and parallel [22–26] tempering.

Given several distributions collected at different thermodynamic states, WHAM obtains the optimal estimate of the free energies of the states. This problem arises in the calculation of potentials of mean force and a variety of free energy difference methods. The central idea of WHAM is to find an optimal estimate of the density of states, or the unbiased distribution, which then allows the free energies to be evaluated as weighted integrals. The optimal density of states is computed from a weighted average of the reweighted energy histograms (hence the name of the method) from different distribution realisations or trajectories. The weights, however, depend on the free energies, so that the free energies and the density of states must be determined self-consistently.

WHAM can be reformulated [1,17] in the limit of zero histogram bin width as an extension of the Bennett acceptance ratio (BAR) method.[27] This form, adopted by the multistate BAR (MBAR) method,[1] avoids the histogram dependency.[1,6,12]

The straightforward implementation of WHAM or MBAR, in which the equations regarding the free energies are solved

by direct iteration, can suffer from slow convergence in the later stages.[14,16,28] Several remedies have been proposed. [1,14,16,28,29] For example, one may use the Newton–Raphson method, which involves a Hessian-like matrix, although the approach sometimes can be unstable.[1] Other more advanced techniques include the trust region and Broyden–Fletcher–Goldfarb–Shanno (BFGS) methods.[16]

An elegant non-iterative alternative is the statistical-temperature WHAM (ST-WHAM),[28,29] which determines the density of states through its logarithmic derivative, or the statistical temperature. In this way, the method estimates the density of states non-iteratively with minimal approximation. ST-WHAM can be regarded as a refinement of the more approximate umbrella integration method (UIM).[30,31] However, the extension to multidimensional ensembles, e.g. the isothermal-isobaric ensemble, can be numerically challenging.[28]

Here, we discuss a numerical improvement of the implementation of WHAM and MBAR using the method of direct inversion in the iterative subspace (DIIS).[32–36] DIIS shares characteristics with other optimisation techniques which use a limited (non-spanning) basis of vectors which produce the most gain towards the optimum. Although still iterative in nature, this implementation can often improve the rate of convergence significantly in difficult cases.

## 2. Method

### 2.1. WHAM

WHAM is a method of estimating the free energies of multiple thermodynamic states with different parameters, such as temperatures, pressures, etc. Below, we shall first review WHAM in

the particular case of a temperature scan since it permits simpler mathematics without much abstraction. Generalisations to umbrella sampling and other ensembles are discussed afterwards.

Consider  $K$  temperatures, labelled by  $\beta = 1/(k_b T)$ , as  $\beta_1, \dots, \beta_K$ . Suppose we have performed the respective canonical (NVT) ensemble simulations at the  $K$  temperatures, and we wish to estimate the free energies at those temperatures. In WHAM, we first estimate the density of states,  $g(E) = \int \delta(\mathcal{E}(\mathbf{x}) - E) d\mathbf{x}$ , as the number density of configurations,  $\mathbf{x}$ , with energy  $E$ , from

$$g(E) = \frac{\sum_{k=1}^K n_k(E)}{\sum_{k=1}^K N_k \exp(-\beta_k E)/Z_k}, \quad (1)$$

where  $n_k(E)$  is the unnormalised energy distribution observed from trajectory  $k$ , which is usually estimated from the energy histogram as the number of independent trajectory frames whose energies fall in the interval  $(E - \Delta E/2, E + \Delta E/2)$  divided by  $\Delta E$  (we shall omit ‘independent’ below for simplicity); thus,  $n_k(E)/N_k$  is the normalised distribution with  $N_k$  being the total number of trajectory frames from simulation  $k$ ; and finally,

$$\exp(-f_k) = Z_k = \int g(E) \exp(-\beta_k E) dE, \quad (2)$$

with  $f_k$  and  $Z_k$  being the dimensionless free energy and partition function, respectively.

To understand Equation (1), we first observe from the definition the single histogram estimate

$$g(E) = \frac{n_k(E)}{d_k(E)} \quad \text{for } k = 1, \dots, K, \quad (3)$$

where  $d_k(E) \equiv N_k \exp(-\beta_k E + f_k)$ . That is, the observed distribution,  $n_k(E)/N_k$ , should roughly match the exact one,  $g(E) w_k(E)$ , where  $w_k(E) \equiv \exp(-\beta_k E + f_k)$  is the normalised weight of the canonical ensemble. The values of Equation (3) from different  $k$  can be combined to improve the precision, and Equation (1) is the optimal combination.[4,5,7,12,13] To see this, recall that in an optimal combination, the relative weight is inversely proportional to the variance. Assuming a Poisson distribution so that  $\text{var}(n_k \Delta E) \approx \langle n_k \rangle \Delta E$ , we have  $\text{var}(n_k \Delta E/d_k) \approx \langle n_k \rangle \Delta E/d_k^2 \propto 1/d_k$  (here,  $\langle \dots \rangle$  means an ensemble average). Averaging the values from Equation (3) using  $(1/d_k)^{-1}$  as the relative weight yields Equation (1).<sup>1</sup> Since for a fixed  $E$ ,  $d_k(E)$  is proportional to  $\langle n_k(E) \rangle$ , several variants of WHAM may be derived using  $n_k(E)$  in place of  $d_k(E)$  as the relative weight for  $g(E)$  [37] or related quantities.[7,28,31,38,39]

From Equations (1) and (2), we find that  $f_i$  satisfies

$$\begin{aligned} f_i &= -\log \int \frac{\sum_{k=1}^K n_k(E) \exp(-\beta_i E)}{\sum_{k=1}^K N_k \exp(-\beta_k E + f_k)} dE \\ &\equiv -\log \mathcal{Z}_i(\mathbf{f}), \end{aligned} \quad (4)$$

where  $\mathcal{Z}_i(\mathbf{f})$  denotes the integral on the right-hand side as a function of  $\mathbf{f} = (f_1, \dots, f_K)$ . Once all  $f_i$  and  $g(E)$  are determined, the free energy at a temperature not simulated,  $\beta$ , can be found from Equation (2) by substituting  $\beta$  for  $\beta_k$ .

### 2.1.1. Histogram-free form

The histogram dependency of WHAM [in using  $n_k(E)$ ] can be avoided by noticing from definition that [12]

$$n_k(E) = \sum_{\mathbf{x}}^{(k)} \delta(\mathcal{E}(\mathbf{x}) - E), \quad (5)$$

where,  $\mathcal{E}(\mathbf{x})$  is the energy function, and  $\sum_{\mathbf{x}}^{(k)}$  denotes a sum over trajectory frames of simulation  $k$ . Using Equation (5) in Equation (4) yields the histogram-free, or the MBAR, form [1,6,12,17]:

$$f_i = -\log \sum_{j=1}^K \sum_{\mathbf{x}}^{(j)} \frac{q_i(\mathbf{x})}{\sum_{k=1}^K N_k q_k(\mathbf{x}) \exp(f_k)}. \quad (6)$$

where  $q_i(\mathbf{x}) \equiv \exp[-\beta_i \mathcal{E}(\mathbf{x})]$ . The  $K = 2$  case is the BAR result,[27] and Equation (6) also holds for a general setting, which permits, e.g. a non-linear parameter dependence (see Appendix 1 for derivation). In this sense, MBAR is not only the zero-bin-width limit of WHAM,[1,17] but also a generalisation. [1] As we shall see, the structural similarity of Equations (4) and (6) allows our acceleration technique to be applicable to both cases. Since both Equations (4) and (6) are invariant under  $f_i \rightarrow f_i + c$  for all  $i$  and an arbitrary  $c$ ,  $f_i$  are determined only up to a constant shift.

### 2.1.2. Extensions to umbrella sampling

We briefly mention a few extensions. First, for a general Hamiltonian with a linear bias

$$\mathcal{H}(\mathbf{x}; \lambda_i) = \mathcal{H}_0(\mathbf{x}) + \lambda_i \mathcal{W}(\mathbf{x}),$$

such that  $q_i(\mathbf{x}) = \exp[-\mathcal{H}(\mathbf{x}; \lambda_i)]$ , we can show, by inserting  $1 = \int \delta(\mathcal{W}(\mathbf{x}) - W) dW$  into Equation (6), that

$$f_i = -\log \int \frac{\sum_{k=1}^K n_k(W) \exp(-\lambda_i W)}{\sum_{k=1}^K N_k \exp(-\lambda_k W + f_k)} dW,$$

where  $n_k(W) \equiv \sum_{\mathbf{x}}^{(k)} \delta(\mathcal{W}(\mathbf{x}) - W)$  is understood to be the unnormalised distribution of the bias  $\mathcal{W}(\mathbf{x})$ . Equation (4) is the special case of  $\mathcal{H}_0(\mathbf{x}) = 0$ ,  $\mathcal{W}(\mathbf{x}) = \mathcal{E}(\mathbf{x})$ , and  $\lambda_i = \beta_i$ . Another common example is a system under a quadratic restraint (umbrella)  $\mathcal{E}_i = \mathcal{E}_0 + \frac{1}{2} A (\xi - \lambda_i)^2$  for some reaction coordinate  $\xi \equiv \xi(\mathbf{x})$ . In this case,  $\mathcal{H}_0(\mathbf{x}) = \beta(\mathcal{E}_0 + \frac{1}{2} A \xi^2)$ , and  $\mathcal{W}(\mathbf{x}) = -\beta A \xi$ . The configuration independent term,  $\frac{1}{2} \beta A \lambda_i^2$ , can be added back to  $f_i$  after the analysis.

### 2.1.3. Extensions to other ensembles

Further,  $\lambda_i$  and  $W$  can be generalised to vectors as  $\lambda_i$  and  $\mathbf{W}$ , respectively. For example, for simulations on multiple isothermal-isobaric ( $NpT$ ) ensembles with different temperatures and pressures, we set  $\lambda_i = (\beta_i, \beta_i p_i)$  and  $\mathbf{W} = (E, V)$  with  $p_i$  and  $V$  being the pressure and volume, respectively. However, if the vector dimension is high, or if the Hamiltonian  $\mathcal{H}(\mathbf{x}; \lambda_i)$  depends non-linearly on  $\lambda_p$ , the histogram-free form, Equation (6), is more convenient.[1] Besides, the factor  $\exp(-\beta_i E)$  can be replaced by a non-Boltzmann (e.g. the multicanonical, [40–42] Tsallis [43],



microcanonical [44,45]) weight for multiple non-canonical simulations.[28]

#### 2.1.4. Solution by iteration

Numerically, the  $f_i$  are most often determined by treating Equation (4) as an iterative equation,

$$f_i^{(new)} = -\log \mathcal{Z}_i(f_i^{(old)}).$$

However, this approach, referred to as direct WHAM below, can take thousands of iterations to finish [14,16,28] (cf. Appendix 2). In Sections 2.3 and 2.4, we give a numerical technique to accelerate the solution of Equation (4) or (6).

### 2.2. ST-WHAM and UIM

For comparison, we briefly discuss two non-iterative alternatives, ST-WHAM [28,29] and UIM.[30,31] By taking the logarithmic derivative of the denominator of Equation (1), we get,

$$\frac{d}{dE} \log \sum_{k=1}^K d_k(E) = -\frac{\sum_{k=1}^K d_k(E) \beta_k}{\sum_{k=1}^K d_k(E)} = -\frac{\sum_{k=1}^K n_k(E) \beta_k}{\sum_{k=1}^K n_k(E)},$$

where we have used Equation (3) to make the final expression independent of  $d_k(E)$ , hence  $f_k$ . So

$$g(E) = \left[ \sum_{k=1}^K n_k(E) \right] \exp \left[ \int^E \frac{\sum_{k=1}^K n_k(E') \beta_k}{\sum_{k=1}^K n_k(E')} dE' \right].$$

This is the ST-WHAM result. In evaluating the integral, we may encounter an empty bin with  $\sum_{k=1}^K n_k(E') \Delta E = 0$ , which leaves the integrand indeterminate. An expedient fix is to let the integrand borrow the value from the nearest non-empty bin [note, however, setting the integrand to zero would cause a larger error in  $g(E)$ ]. ST-WHAM is most convenient in one dimension, and its results usually differ only slightly from those of WHAM.[28] In UIM, [30,31] the distribution  $n_k(E)$  is further approximated as a Gaussian. We note that ST-WHAM is difficult when we have more thermodynamic variables in the ensemble of interest. Below we show that WHAM with the DIIS method can handle such a case for the Lennard-Jones (LJ) fluid, readily.

### 2.3. DIIS

DIIS is a technique useful for solving equations, [32–36] and we use it to solve Equation (4) here. A schematic illustration is shown in Figure 1. We first represent an approximate solution by a trial vector,  $\mathbf{f} = (f_1, \dots, f_K)$ , which is, in our case, the vector of the dimensionless free energies. The target equations can be written as

$$R_i(\mathbf{f}) = 0 \quad \text{for } i = 1, \dots, K, \quad (7)$$

which is  $-\log \mathcal{Z}_i(\mathbf{f}) - f_i$  in our case. The left-hand side of Equation (7) also forms a  $K$ -dimensional vector,  $\mathbf{R} = (R_1, \dots, R_K)$ , which is referred to as the residual vector. The magnitude  $\|\mathbf{R}\|$  represents the error, and  $\mathbf{R}(\mathbf{f})$  should optimally point in a direction that reduces the error of  $\mathbf{f}$ .

If Equation (7) is solved by direct iteration,  $\mathbf{f}$  is replaced by  $\mathbf{f} + \mathbf{R}(\mathbf{f})$  in each time. This can be a slow process because the

residual vector  $\mathbf{R}$  does not always have the proper direction and/or magnitude to bring  $\mathbf{f}$  close to the true solution  $\mathbf{f}^*$ . The magnitude of  $\mathbf{R}$ , however, can be used as a reliable measure of the error of  $\mathbf{f}$ . Thus, in DIIS, we try to find a vector  $\hat{\mathbf{f}}$  with minimal error  $\|\mathbf{R}(\hat{\mathbf{f}})\|$ , which would be more suitable for direct iteration.

Suppose now we have a basis of  $M$  trial vectors  $\mathbf{f}_1, \dots, \mathbf{f}_M$  (where  $M$  can be much less than  $K$ ), and the residual vectors are  $\mathbf{R}_1, \dots, \mathbf{R}_M$  [where  $\mathbf{R}_j \equiv \mathbf{R}(\mathbf{f}_j)$  for  $j = 1, \dots, M$ ], respectively. We wish to construct a vector  $\hat{\mathbf{f}}$  with minimal error from a linear combination of the trial vectors. To do so, we first find the combination of the residual vectors  $\hat{\mathbf{R}} = \sum_{i=1}^M c_i \mathbf{R}_i$  that minimises the error  $\|\hat{\mathbf{R}}\|$  under the constraint

$$\sum_{i=1}^M c_i = 1. \quad (8)$$

Mathematically, this means that we solve for the  $c_i$  simultaneously from Equation (8) and

$$\sum_{j=1}^M (\mathbf{R}_i \cdot \mathbf{R}_j) c_j = \lambda, \quad (9)$$

for all  $i$ , with  $\lambda$  being an unknown Lagrange multiplier that is to be determined ~~from~~ along with  $c_i$ . Now the corresponding combination of the trial vectors,  $\hat{\mathbf{f}} = \sum_{i=1}^M c_i \mathbf{f}_i$  should be close to the desired minimal-error vector. This is because around the true solution  $\mathbf{f}^*$ , Equation (7) should be nearly linear; so the residual vector

$$\mathbf{R}(\hat{\mathbf{f}}) = \mathbf{R} \left( \sum_{i=1}^M c_i \mathbf{f}_i \right) \approx \sum_{i=1}^M c_i \mathbf{R}(\mathbf{f}_i) = \hat{\mathbf{R}},$$

has the minimal magnitude. In other words,  $\hat{\mathbf{f}}$ , among all linear combinations of  $\{\mathbf{f}_i\}$ , is the closest to the true solution, under the linear approximation. Thus, an iteration based on  $\hat{\mathbf{f}}$  should be efficient.

With  $M = K + 1$  independent ~~bases~~, one can show that it is possible to find a combination with zero  $\hat{\mathbf{R}}$ , which means that  $\hat{\mathbf{f}}$  would be the true solution if the equations were linear. A particularly instructive case is that of two vectors ( $M = 2$ ) in one dimension ( $K = 1$ )<sup>2</sup>. We then recover the secant method, [46], as shown in Figure 1(d). The number of bases,  $M$ , however, should not exceed  $K + 1$  (or, in our case,  $K$  because of the arbitrary shift constant of  $f_i$ ) to keep Equations (9) independent, although this restriction may be relaxed using certain numerical techniques. [46]

We now construct a new trial vector  $\mathbf{f}^{(n)}$  as

$$\mathbf{f}^{(n)} = \hat{\mathbf{f}} + \alpha \mathbf{R}(\hat{\mathbf{f}}),$$

where the factor  $\alpha$  is 1.0 in this study (although a smaller value is recommended for other applications.[35,36]) The new vector  $\mathbf{f}^{(n)}$  is used to update the basis as shown next.

### 2.4. Basis updating

In each iteration of DIIS, the basis is updated by the new trial vector  $\mathbf{f}^{(n)}$  from the above step. Initially, the basis contains a single vector. As we add more vectors into the basis in subsequent

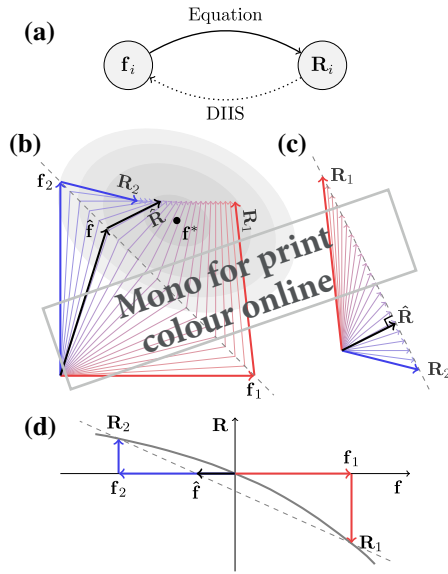


**Figure 1.** Schematic illustrations of the method of direct inversion of the iterative subspace (DIIS). Notes: (a) As an iterative method, DIIS solves the equation,  $R(f) = 0$ , by a feedback loop. When the equation is applied to a trial solution, represented by vector  $f_i$ , we get a residual vector  $R_i \equiv R(f_i)$ , whose magnitude indicates the error. Ideally, if  $f_i$  were the true solution,  $R_i$  would be zero. In the feedback step, we correct  $f_i$  using  $R_i$ . The task of DIIS is to construct from a few previous vectors accumulated during the iteration an optimal trial vector  $\hat{f}$  with hopefully the smallest error  $\|\hat{R}\|$  to help the next round of iteration. (b) and (c) Given a basis of  $M$  (two here) trial vectors, DIIS seeks the combination  $\hat{R} = \sum_{i=1}^M c_i R_i$  that minimises the magnitude  $\|\hat{R}\|$  under the constraint  $\sum_{i=1}^M c_i = 1$  [panel (c)]. The corresponding combination of the trial vectors,  $\hat{f} = \sum_{i=1}^M c_i f_i$ , is expected to be close to true solution,  $f^*$ . Then, we construct the new trial vector as  $f^{(n)} = \hat{f} + \hat{R}$  and use it to update the basis for the next round of iteration. (d) If the vectors are one-dimensional (i.e. scalars), it is possible to find a vanishing  $\hat{R}$ , and DIIS is equivalent to the secant method.

iterations, some old vectors may be removed to maintain a convenient and efficient maximal size of  $M$ .

A simple updating scheme [35] is to treat the basis as a queue: we add  $f^{(n)}$  to the basis, if the latter contains fewer than  $M$  vectors, or substitute  $f^{(n)}$  for the earliest vector in the basis. If, however,  $f^{(n)}$  produces an error greater than  $K_r$  times the error of  $f_{\min}^{(n)}$ , the least erroneous vector in the basis, we rebuild the basis from  $f_{\min}^{(n)}$ . Here, the error of a vector  $f$  is defined as  $\|R(f)\|$ , and  $K_r = 10.0$  is recommended. [35]

We used the following modification in this study. First, we find the most erroneous vector,  $f_{\max}^{(n)}$ , from the basis. If the new vector,  $f^{(n)}$ , produces an error less than  $f_{\max}^{(n)}$ , we add  $f^{(n)}$  into the basis or, if the basis is full, substitute  $f^{(n)}$  for  $f_{\max}^{(n)}$ . Otherwise, we remove  $f_{\max}^{(n)}$  from the basis, and if this empties the basis, we rebuild the basis from  $f^{(n)}$ .

Since the DIIS process is reduced to the direct iteration if  $M = 1$ , the method is effective only if multiple basis vectors are used.

### 3. Results

We tested DIIS WHAM and MBAR on three systems: Ising model, LJ fluid, and the villin headpiece (a small protein) in aqueous solution (see Sections 3.2, 3.3, and 3.4, respectively, for details). We tuned the parameters such that direct WHAM and MBAR would take thousands of iterations to finish.

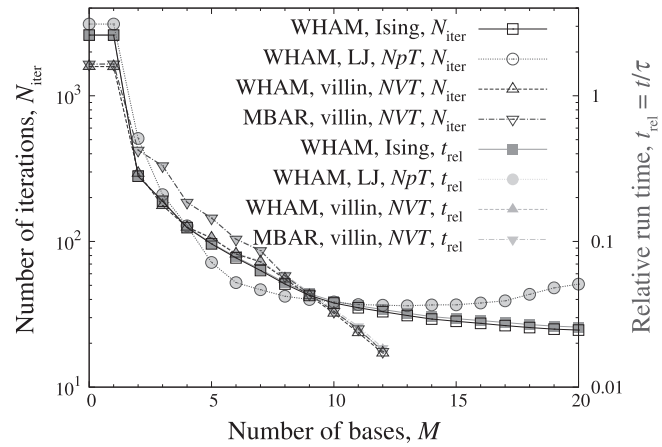


**Figure 2.** Number of iterations and run time versus the number of bases,  $M$ , in DIIS. Notes: The four test cases are (1) WHAM on the Ising model, (2) WHAM on the LJ fluid in the  $NpT$  ensemble, (3) WHAM on the mini-protein villin headpiece in the NVT ensemble (with the bin width of energy histograms being 1.0) and (4) MBAR on the same protein system. The  $M = 0$  points represent direct WHAM. The run times are inversely scaled by a factor  $\tau$  for better alignment with the numbers of iterations. The scaling factors  $\tau$  for cases 1–4 are  $12.5$ ,  $1.87 \times 10^3$ ,  $14.3$  and  $260$  seconds, respectively. The results were averaged over independent samples for the Ising model and LJ fluid. For the villin headpiece, the results were averaged over bootstrap [4,15,47] samples for WHAM, or over random subsamples with about 1% of the trajectory frames for MBAR. To mimic the correlation in the trajectories, each data point in the bootstrap sample is either randomly drawn from the trajectory, or the same as the previous one (if any) with probability  $\exp(-\Delta t_m D / t_a c t)$ , where  $\Delta t_m D$  and  $t_a c t$  are the time step of molecular dynamics and the autocorrelation time of the potential energy, respectively. Here, the error tolerance  $\max\{|R_i|\}$  is  $10^{-8}$ . The lines are a guide for the eyes.

The main results are summarised in Figure 2, from which one can see that DIIS can speed up WHAM and MBAR dramatically in these cases. The real run time roughly matched the number of iterations, suggesting a negligible overhead for using DIIS. This is unsurprising, for it is often much more expensive to compute the right-hand side of Equation (4) or (6).

#### 3.1. Set-up

For simplicity, we assumed equal autocorrelation times from different temperatures (and pressures). The approximation should not affect the convergence behaviour of the methods.

In testing WHAM and MBAR, the initial free energies were obtained from the single histogram method:

$$\Delta f_i = \log \langle \exp(\Delta \beta_i E) \rangle_{i+1},$$

where  $\Delta A_i \equiv A_{i+1} - A_i$  for any quantity  $A$ , and  $\langle \dots \rangle_{i+1}$  denotes an average over trajectory  $i + 1$ . Then,  $f_i = f_1 + \sum_{j=1}^{i-1} \Delta f_j$ . Iterations are continued until all  $|R_i|$  are reduced below a certain value.

For comparison, we also computed  $f_i$  from three approximate formulae. The first is [16,48]

$$\Delta f_i \approx \overline{\langle E \rangle}_i \Delta \beta_i, \quad (10)$$

where  $\overline{A}_i \equiv (A_{i+1} + A_i)/2$ . The second is an improvement by the Euler–Maclaurin expansion [49–52]:

$$\Delta f_i \approx \overline{\langle E \rangle}_i \Delta \beta_i + (\langle \delta E^2 \rangle_{i+1} - \langle \delta E^2 \rangle_i) \frac{\Delta \beta_i^2}{12}, \quad (11)$$

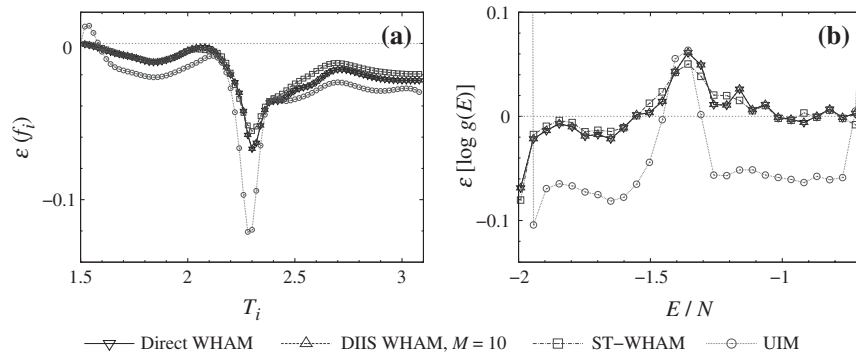


**Figure 3.** Errors of (a) the dimensionless free energies,  $f_i$ , and (b) the logarithmic density of states,  $\log g(E)$ , for the  $N = 64 \times 64$  two-dimensional Ising model (plotted with an energy spacing of 200). Here,  $\epsilon(a) \equiv a - a^{\text{ref}}$ , and the reference values for  $f_i$  and  $g(E)$  were computed using the methods in Refs. [53] and [54], respectively. The bin size of the energy histograms is  $\Delta E = 4$ . Lines are a guide for the eyes.

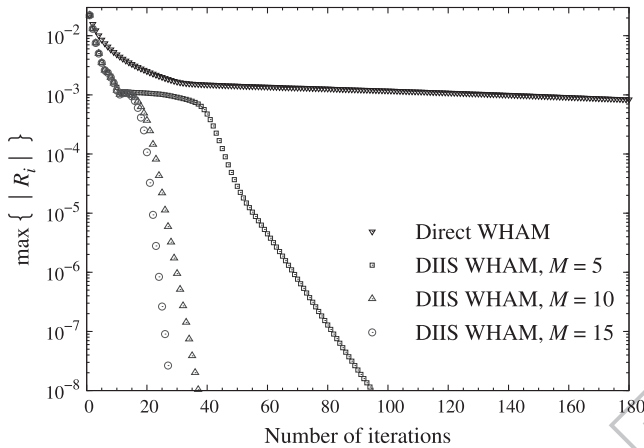


**Figure 4.** Convergence error,  $\max\{|R_i|\}$ , versus the number of iterations in direct and DIIS WHAMs for the  $64 \times 64$  two-dimensional Ising model. Results were geometrically averaged over independent samples.

where  $\langle \delta E^2 \rangle_k \equiv \langle (E - \langle E \rangle_k)^2 \rangle_k$  for  $k = i$  and  $i + 1$ . The third formula is derived from the same expansion but using  $E$  instead of  $\beta$  as the independent variable (after integration by parts,  $\int E d\beta = E\beta - \int \beta dE$ ):

$$\Delta f_i \approx \overline{\langle E \rangle}_i \Delta \beta_i - (\langle \delta E^2 \rangle_{i+1}^{-1} - \langle \delta E^2 \rangle_i^{-1}) \frac{(\Delta \langle E \rangle_i)^2}{12}. \quad (12)$$

### 3.2. Ising model

The first system is a  $64 \times 64$  Ising model. We used parallel tempering [22–26] Monte Carlo (MC) for eighty temperatures:  $T = 1.5, 1.52, \dots, 3.08$ ,

To study the accuracy, we generated a large sample with  $10^9$  single-site MC steps for each temperature. Figure 3 shows that DIIS and direct WHAMs produced identical dimensionless free energies. The differences between the ST-WHAM and WHAM results were subtle, whereas the approximate UIM produced more deviation in the results, especially around the critical region.

To study the rate of convergence, we generated independent samples with  $10^7$  MC steps at each temperature. Figure 4 shows a faster decay of the error in DIIS WHAM than in direct WHAM.

### 3.3. LJ fluid

We tested the DIIS method on the 256-particle LJ fluid in the isothermal-isobaric ( $NpT$ ) ensemble. This is a case for the two-dimensional ( $p$  and  $T$ ) WHAM, which can be difficult for ST-WHAM. [28] The potential interaction between particles was cut-off at half the box size. We simulated the system using parallel tempering MC. We considered the system at  $N_T \times N_p = 6 \times 3$  conditions, with temperatures  $T = 1.2, 1.3, \dots, 1.7$ , and pressures  $p = 0.1, 0.15, 0.2$ . The bin sizes for energy and volume were 1.0 and 2.0, respectively.

As shown in Figure 2, DIIS WHAM effectively reduced the run time, although the efficiency of DIIS does not always increase with the number of basis set members,  $M$ .

### 3.4. Villin headpiece

We tested the methods on a small protein, the villin headpiece (PDB ID: 1VII), in aqueous solution. This is a well-known test system. [55] The protein was immersed in a dodecahedron box with 1898 TIP3P water molecules and two chloride ions. The force field was AMBER99SB [56,57] with the side-chain modifications. [58] Molecular dynamics (MD) simulations were performed using GROMACS 5.0, [59–65] with a time step of 2 fs. Velocity rescaling [66] was used as the thermostat with the time constant being 0.1 ps. The electronic interaction was handled by the particle mesh Ewald method. [67] The constraints were handled by the LINCS method [68] for hydrogen-related chemical bonds on the protein and by the SETTLE method [69] for water molecules.

We simulated the system at 12 temperatures  $T = 300$  K, 310 K, ..., 410 K, each for approximately 200 ns. The energy distributions were properly overlapped, as shown in Figure 5(e). The energies of individual trajectory frames were saved every 0.1 ps, so that there were about two million frames for analysis at each temperature.

As shown in Figure 2, direct WHAM suffered from slow convergence, while the DIIS methodology again delivered a speed-up of two orders of magnitude, in the number of iterations or in real time. The MBAR case was similar, although MBAR was slower than WHAM as it did not use histogram to aggregate data.



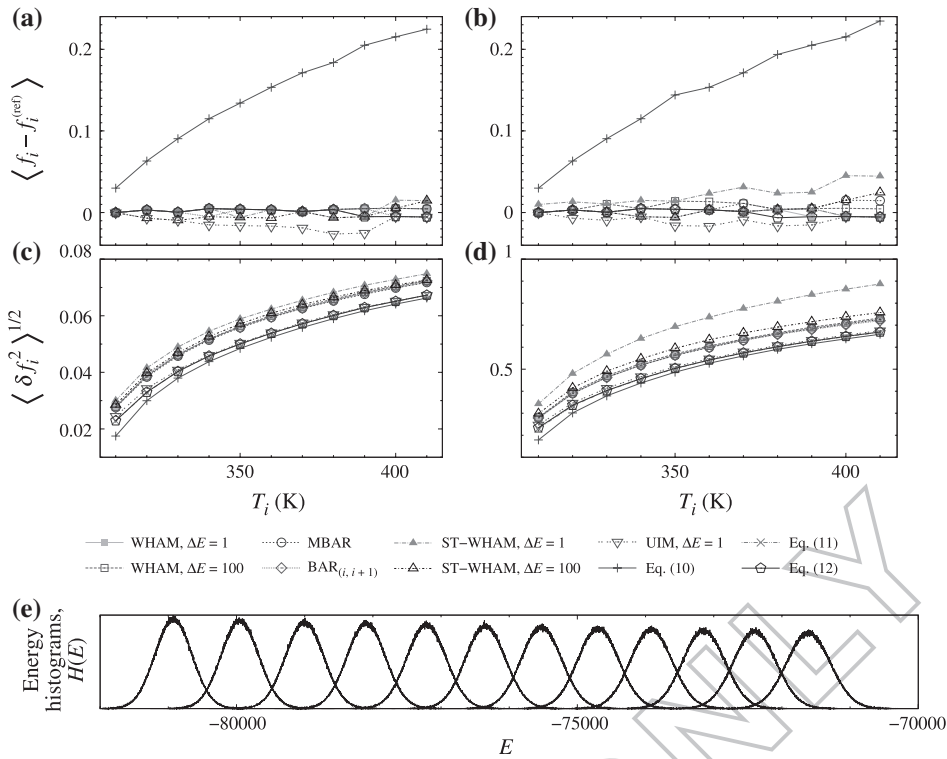


**Figure 5.** Accuracy [(a) and (c)] and precision [(b) and (d)] of the dimensionless free energies,  $f_i$ , from WHAM, BAR, ST-WHAM, UIM and approximate formulae for the villin headpiece in solution. Notes: Two types of samples were used. A large sample [(a) and (b)] and a small sample [(c) and (d)] contain roughly 1% and 0.01% of all trajectory frames, respectively. The results were averaged over random samples. The MBAR results computed from all trajectory frames were used as the reference.  $f_i$  at  $T = 300$  K is fixed at zero. The lines are a guide for the eyes. (e) Energy histograms collected with bin width  $\Delta E = 1.0$ .

To compare the errors of the methods, we prepared two types of samples of different sizes. A larger sample was randomly selected from roughly  $r = 1\%$  of all trajectory frames from every temperature. In a smaller one,  $r$  was reduced to 0.01%. The reference values of  $f_i$  were computed from all trajectory frames using MBAR, which is the zero-bin-width limit of WHAM. [1,17] In terms of accuracy [Figures 5(a) and 5(c)], WHAM, MBAR, BAR, ST-WHAM, Equations (11) and (12) were comparably good; UIM was slightly inferior for the larger sample; Equation (10) was the worst. The accuracy was largely independent of the sample size. In terms of precision [Figures 5(b) and 5(d)], the differences were small. Generally, WHAM was insensitive to the bin size, whereas ST-WHAM was slightly affected by a small bin size for the smaller samples.

#### 4. Conclusions

In this work, we showed that the DIIS technique can often significantly accelerate WHAM and MBAR to produce free energy difference. The technique achieves rapid convergence by an optimal combination of the approximate solutions obtained during iteration. DIIS does not require computing the Hessian-like matrix,  $-\partial R(f)/\partial f$ , and is numerically stable with minimal run time overhead. Compared to other advanced techniques, [1,16] DIIS is relatively simple and easy to implement. However, methods based on Hessian matrices may further accelerate the solution process for final stages. Other related free energy methods [7,37–39] may also benefit from this technique.

There are some non-iterative alternatives to WHAM, although they may be less general and/or accurate in some aspect. The use of DIIS makes scanning more than one thermodynamic state variable or a non-linear variable computationally convenient. This was demonstrated here in the  $NpT$  LJ fluid case. Problems with only one thermodynamic variable to scan, such as temperature, are amenable to the non-iterative ST-WHAM, or the more approximate UIM.

#### Notes

1. We can also view Equation (1) as the result of applying Equation (3) to the composite ensemble of the  $K$  canonical ensembles, [13] using the following substitutions:  $n_k(E) \rightarrow \sum_{k=1}^K n_k(E)$ ,  $N_k \rightarrow \sum_{k=1}^K N_k \equiv N_{tot}$ , and  $w_k(E) \rightarrow \sum_{k=1}^K (N_k/N_{tot}) w_k(E)$ . The last expression is the normalised ensemble weight in the composite ensemble. Note that the composite ensemble is closely related to the expanded ensemble that underlies the simulated tempering method. [20,21] However, in the latter case, one can show that the  $N_k$  in Equation (1) should be replaced by the average,  $\langle N_k \rangle$ , and the combination  $\langle N_k \rangle / Z_k$  is proportional to the weight  $\exp(\eta_k)$  in the acceptance probability of temperature transitions,  $A(\beta_k \rightarrow \beta_{k'}) = \min\{1, \exp[\eta_{k'} - \eta_k - (\beta_{k'} - \beta_k) E]\}$ . This variant is thus more convenient as it depends only on the known weight,  $\eta_k$ , instead of on the unknown  $f_k$ .
2. This is the case for solving the BAR equation, because  $f_i$  are determined up to a constant shift, the virtual dimension is 1.
3. We can also show Equation (A2) by considering the composite ensemble of the  $K$  states. The number of visits to a phase-space element at  $\mathbf{y}$  is given by the product of the total sample size,  $N_{tot} = \sum_{k=1}^K N_k$ , the distribution of the composite ensemble

$w_i^{\text{tot}} = \sum_{k=1}^K (N_k/N_i^{\text{tot}}) w_k(\mathbf{y})$ , and the volume  $d\mathbf{y}$ . This gives  $g(\mathbf{y}) \sum_{k=1}^K N_k q_k(\mathbf{y})/Z_k[g] d\mathbf{y}$ , and it is expected to match the observed number of visits to the element,  $\sum_{j=1}^K \sum_{\mathbf{x}} \delta(\mathbf{x} - \mathbf{y}) d\mathbf{y}$ , regardless of the state  $j$ .

4. For  $A_{12}$ , we set  $E_c = -\Delta\beta/(2a)$ , and  $D(E;f^*) = \exp\left(\frac{1}{2}\Delta\beta E\right)J(E)$ , with

$$\begin{aligned} J(E) &\equiv 2 \cosh\left(\frac{1}{2}\Delta\beta E\right) + \exp\left(-\frac{3}{2}\Delta\beta E - \frac{1}{a}\Delta\beta^2\right) \\ &\approx 2 \cosh\left(\frac{1}{2}\Delta\beta E\right) + \exp\left(-\frac{u\Delta\beta^2}{4a}\right) \\ &\approx 2\theta \exp\left(\frac{\Delta\beta^2 E^2}{8\theta}\right) / \left[1 + \frac{(3-\theta)\Delta\beta^4 E^4}{24\cdot 2^4 \cdot \theta^2}\right], \end{aligned}$$

where  $\theta = 1 + \frac{1}{2} \exp[-u\Delta\beta^2/(4a)]$ . The parameter  $u$  should be  $5/2$  to match the small  $\Delta\beta$  behaviour, although the overall accuracy can be improved by a value of  $u \approx 2.11$ .

## Acknowledgements

It is a pleasure to thank Dr. Y. Zhao, J. A. Drake, Dr. M. R. Shirts, Dr. M. W. Deem, Dr. J. Ma, Dr. J. Perkyns and Dr. G. Lynch for helpful discussions.

## Disclosure statement

No potential conflict of interest was reported by the authors.

## Funding

This work was supported by the National Science Foundation (CHE-1152876), the National Institutes of Health (GM037657), and the Robert A. Welch Foundation (H-0037). Computer time on the Lonestar supercomputer at the Texas Advanced Computing Center at the University of Texas at Austin is gratefully acknowledged.

## References

- Shirts MR, Chodera JD. Statistically optimal analysis of samples from multiple equilibrium states. *J Chem Phys.* 2008;129:124105.
- Ferrenberg AM, Swendsen RH. New monte-carlo technique for studying phase transitions. *Phys Rev Lett.* 1988;61:2635–2638.
- Ferrenberg AM, Swendsen RH. Optimized monte-carlo data analysis. *Phys Rev Lett.* 1989;63:1195–1198.
- Newman E, Barkema G. Monte-carlo methods in statistical physics. 1st ed. Oxford: Clarendon Press; 1999.
- Frenkel D, Smit B. Understanding molecular simulation, second edition: from algorithms to applications (computational science). 2nd ed. Academic Press; 2001.
- Kumar S, Rosenberg JM, Bouzida D, et al. The weighted histogram analysis method for free-energy calculations on biomolecules. i. the method. *J Comput Chem.* 1992;13:1011–1021.
- Roux B. The calculation of the potential of mean force using computer simulations. *Comput Phys Commun.* 1995;91:275–282.
- Bartels C, Karplus M. Multidimensional adaptive umbrella sampling: applications to main chain and side chain peptide conformations. *J Comput Chem.* 1997;18:1450–1462.
- Galluccio E, Andrec M, Felts AK, et al. Temperature weighted histogram analysis method, replica exchange, and transition paths. *J Phys Chem B.* 2005;109:6722–6731.
- Habeck M. Bayesian reconstruction of the density of states. *Phys Rev Lett.* 2007;98:200601.
- Habeck M. Bayesian estimation of free energies from equilibrium simulations. *Phys Rev Lett.* 2012;109:100601.
- Souaille M, Roux B. Extension to the weighted histogram analysis method: combining umbrella sampling with free energy calculations. *Comput Phys Commun.* 2001;135:40–57.
- Chodera JD, Swope WC, Pitera JW, et al. Use of the weighted histogram analysis method for the analysis of simulated and parallel tempering simulations. *J Chem Theory Comput.* 2007;3:26–41.
- Bereau T, Swendsen RH. Optimized convergence for multiple histogram analysis. *J Comput Phys.* 2009;228:6119–6129.
- Hub JS, de Groot BL, van der Spoel D. g-wham-a free weighted histogram analysis implementation including robust error and autocorrelation estimates. *J Chem Theory Comput.* 2010;6:3713–3720.
- Zhu F, Hummer G. Convergence and error estimation in free energy calculations using the weighted histogram analysis method. *J Comput Chem.* 2012;33:453–465.
- Tan Z, Galluccio E, Lapelosa M, et al. Theory of binless multi-state free energy estimation with applications to protein-ligand binding. *J Chem Phys.* 2012;136:144102.
- Torrie GM, Valleau JP. Monte-carlo free energy estimates using non-boltzmann sampling: Application to the sub-critical lennard-jones fluid. *Chem Phys Lett.* 1974;28:578–581.
- Laio A, Parrinello M. Escaping free-energy minima. *Proc Natl Acad Sci.* 2002;99:12562–12566.
- Marinari E, Parisi G. Simulated tempering: a new monte-carlo scheme. *EPL (Europhys Lett).* 1992;19:451.
- Lyubartsev AP, Martsinovski AA, Shevkunov SV, et al. New approach to monte-carlo calculation of the free energy: Method of expanded ensembles. *J Chem Phys.* 1992;96:1776–1783.
- Swendsen RH, Wang JS. Replica monte-carlo simulation of spin-glasses. *Phys Rev Lett.* 1986;57:2607–2609.
- Geyer CJ. In: Proceedings of the 23rd Symposium on the Interface. New York (NY): American Statistical Association; 1991. p. 156.
- Hukushima K, Nemoto K. Exchange monte-carlo method and application to spin glass simulations. *J Phys Soc Jpn.* 1996;65:1604–1608.
- Hansmann UHE. Parallel tempering algorithm for conformational studies of biological molecules. *Chem Phys Lett.* 1997;281:140–150.
- Earl DJ, Deem MW. Parallel tempering: theory, applications, and new perspectives. *Phys Chem Chem Phys.* 2005;7:3910–3916.
- Bennett CH. Efficient estimation of free energy differences from monte-carlo data. *J Comput Phys.* 1976;22:245–268.
- Kim J, Keyes T, Straub JE. Communication: iteration-free, weighted histogram analysis method in terms of intensive variables. *J Chem Phys.* 2011;135:061103.
- Fenwick MK. A direct multiple histogram reweighting method for optimal computation of the density of states. *J Chem Phys.* 2008;129:125106.
- Kästner J, Thiel W. Bridging the gap between thermodynamic integration and umbrella sampling provides a novel analysis method: umbrella integration. *J Chem Phys.* 2005;123:144104.
- Kästner J. Umbrella integration in two or more reaction coordinates. *J Chem Phys.* 2009;131:034109.
- Pulay P. Convergence acceleration of iterative sequences. the case of scf iteration. *Chem Phys Lett.* 1980;73:393–398.
- Pulay P. Improved scf convergence acceleration. *J Comput Chem.* 1982;3:556–560.
- Hamilton TP, Pulay P. Direct inversion in the iterative subspace (diis) optimization of openshell, excitedstate, and small multiconfiguration scf wave functions. *J Chem Phys.* 1986;84:5728–5734.
- Kovalenko A, Ten-no S, Hirata F. Solution of three-dimensional reference interaction site model and hypernetted chain equations for simple point charge water by modified method of direct inversion in iterative subspace. *J Comput Chem.* 1999;20:928–936.
- Howard J, Pettitt B. Integral equations in the study of polar and ionic interaction site fluids. *J Stat Phys.* 2011;145:441–466.
- Shen J, McCammon J. Molecular dynamics simulation of superoxide interacting with superoxide dismutase. *Chem Phys.* 1991;158:191–198.
- Woolf TB, Roux B. Conformational flexibility of o-phosphorylcholine and o-phosphorylethanolamine: A molecular dynamics study of solvation effects. *J Am Chem Soc.* 1994;116:5916–5926.

- [39] Crouzy S, Woolf T, Roux B. A molecular dynamics study of gating in dioxolane-linked gramicidin channels. *Biophys J*. 1994;67:1370–1386.
- [40] Mezei M. Adaptive umbrella sampling: self-consistent determination of the non-boltzmann bias. *J Comput Phys*. 1987;68:237–248.
- [41] Berg BA, Neuhaus T. Multicanonical ensemble: a new approach to simulate first-order phase transitions. *Phys Rev Lett*. 1992;68:9–12.
- [42] Lee J. New monte-carlo algorithm: entropic sampling. *Phys Rev Lett*. 1993;71:211–214.
- [43] Tsallis C. Possible generalization of boltzmann-gibbs statistics. *J Stat Phys*. 1988;52:479–487.
- [44] Yan Q, de Pablo JJ. Fast calculation of the density of states of a fluid by monte-carlo simulations. *Phys Rev Lett*. 2003;90:035701.
- [45] Martin-Mayor V. Microcanonical approach to the simulation of first-order phase transitions. *Phys Rev Lett*. 2007;98:137207.
- [46] Press WH, Teukolsky SA, Vetterling WT, Flannery BP. Numerical recipes in C. The art of scientific computing. 2nd ed. Cambridge: Cambridge University Press; 1992.
- [47] Efron B. Bootstrap methods: another look at the jackknife. *Ann Stat*. 1979;7:1–26.
- [48] Park S, Pande VS. Choosing weights for simulated tempering. *Phys Rev E*. 2007;76:016703.
- [49] Arfken GB, Weber HJ. Mathematical methods for physicists. 5th ed. Academic Press; 2001.
- [50] Abramowitz M, Stegun I. Handbook of mathematical functions: with formulas, graphs, and mathematical tables. In: *Applied mathematics series*. Dover Publications; 1964.
- [51] Wang Z, DGuo. Special functions. World Scientific; 1989.
- [52] Whittaker ET, Watson GN. A course of modern analysis. 10th ed. Cambridge University Press; 1927.
- [53] Ferdinand AE, Fisher ME. Bounded and inhomogeneous ising models. i. specific-heat anomaly of a finite lattice. *Phys Rev*. 1969;185:832–846.
- [54] Beale PD. Exact distribution of energies in the two-dimensional ising model. *Phys Rev Lett*. 1996;76:78–81.
- [55] Duan Y, Kollman PA. Pathways to a protein folding intermediate observed in a 1-microsecond simulation in aqueous solution. *Science*. 1998;282:740–744.
- [56] Wang J, Cieplak P, Kollman PA. How well does a restrained electrostatic potential (resp) model perform in calculating conformational energies of organic and biological molecules? *J Comput Chem*. 2000;21:1049–1074.
- [57] Hornak V, Abel R, Okur A, et al. Comparison of multiple amber force fields and development of improved protein backbone parameters. *Proteins: Struct, Funct, Bioinf*. 2006;65:712–725.
- [58] Lindorff-Larsen K, Piana S, Palmo K, et al. Improved side-chain torsion potentials for the amber ff99sb protein force field. *Proteins: Struct, Funct, Bioinf*. 2010;78:1950–1958.
- [59] Berendsen H, van der Spoel D, van Drunen R. Gromacs: a message-passing parallel molecular dynamics implementation. *Comput Phys Commun*. 1995;91:43–56.
- [60] Lindahl E, Hess B, van der Spoel D. Gromacs 3.0: a package for molecular simulation and trajectory analysis. *J Mol Model*. 2001;7:306–317.
- [61] Van Der Spoel D, Lindahl E, Hess B, et al. Gromacs: fast, flexible, and free. *J Comput Chem*. 2005;26:1701–1718.
- [62] Hess B, Kutzner C, van der Spoel D, et al. Gromacs 4: algorithms for highly efficient, load-balanced, and scalable molecular simulation. *J Chem Theory and Comput*. 2008;4:435–447.
- [63] Pronk S, Páll S, Schulz R, et al. Gromacs 4.5: a high-throughput and highly parallel open source molecular simulation toolkit. *Bioinformatics*. 2013;29:845–854.
- [64] Páll S, Abraham M, Kutzner C, Hess B, Lindahl E. Tackling exascale software challenges in molecular dynamics simulations with gromacs. Markidis S, Laure E, editors. Solving software challenges for exascale. Lecture notes in computer science; vol. 8759. Springer International Publishing; 2015. p. 3–27.
- [65] Abraham MJ, Murtola T, Schulz R, et al. Gromacs: high performance molecular simulations through multi-level parallelism from laptops to supercomputers. *SoftwareX*. 2015;1–2:19–25.
- [66] Bussi G, Donadio D, Parrinello M. Canonical sampling through velocity rescaling. *J Chem Phys*. 2007;126:014101.
- [67] Essmann U, Perera L, Berkowitz ML, et al. A smooth particle mesh ewald method. *J Chem Phys*. 1995;103:8577–8593.
- [68] Hess B, Bekker H, Berendsen HJC, et al. Lincs: A linear constraint solver for molecular simulations. *J Comput Chem*. 1997;18:1463–1472.
- [69] Miyamoto S, Kollman PA. Settle: an analytical version of the shake and rattle algorithm for rigid water models. *J Comput Chem*. 1992;13:952–962.
- [70] Leonard T, Hsu J. Bayesian methods: an analysis for statisticians and interdisciplinary researchers. In: *Cambridge Series in Statistical and Probabilistic Mathematics*. Cambridge University Press; 1999.
- [71] Duda R, Hart P, Stork D. Pattern classification. 2nd ed. Wiley; 2000.
- [72] Dempster AP, Laird NM, Rubin DB. Maximum likelihood from incomplete data via the em algorithm. *J R Stat Soc, Series B*. 1977;39(1):1–38.
- [73] Neal R, Hinton G. A view of the em algorithm that justifies incremental, sparse, and other variants. *Nato-asi series*; vol. 89. Springer; 1998. p. 355–368.
- [74] Press WH, Teukolsky SA, Vetterling WT, Flannery BP. Numerical recipes in C. The art of scientific computing. 3rd ed. Cambridge: Cambridge University Press; 2007.

## Appendix 1. Probabilistic derivations of Equation (6)

Here we give some derivations of Equation (6). First, we show that Equation (6) is a generalisation of Equation (4) from the energy space to the configuration space. We follow the probabilistic argument, [8,11,16,17] for simplicity. We assume that the system is subject to an unknown underlying configuration-space field,  $g(\mathbf{y})$ , such that the distribution of state  $k$  is  $w_k(\mathbf{y}) \equiv g(\mathbf{y}) q_k(\mathbf{y}) / Z_k[g]$ , with

$$Z_k[g] = \int g(\mathbf{y}) q_k(\mathbf{y}) d\mathbf{y}. \quad (\text{A1})$$

We now seek the most probable  $g(\mathbf{y})$  from the observed trajectory. Given a certain  $g(\mathbf{y})$ , the probability of observing the trajectories,  $\{\mathbf{x}\}$ , is given by

$$p(\{\mathbf{x}\}|g) \propto \prod_{k=1}^K \prod_{\mathbf{x}}^{(k)} \frac{g(\mathbf{x}) q_k(\mathbf{x})}{Z_k[g]}. \quad 100$$

This is also the likelihood of  $g$  given the observed trajectory,  $\{\mathbf{x}\}$ . Thus, to find the most probable  $g(\mathbf{y})$ , we only need to maximise  $\log p(\{\mathbf{x}\}|g)$  by taking the functional derivative with respect to  $g(\mathbf{y})$  and setting it to zero, which yields

$$g(\mathbf{y}) = \frac{\sum_{j=1}^K \sum_{\mathbf{x}} \delta(\mathbf{x} - \mathbf{y})}{\sum_{k=1}^K N_k q_k(\mathbf{y}) / Z_k[g]}, \quad (\text{A2}) \quad 105$$

where we have used  $\delta \log g(\mathbf{x}) / \delta g(\mathbf{y}) = \delta(\mathbf{x} - \mathbf{y}) / g(\mathbf{y})$ , and  $\delta Z_k[g] / \delta g(\mathbf{y}) = q_k(\mathbf{y})$ .<sup>4</sup> Using Equation (A2) in Equation (A1), and then setting  $g$  to 1.0 yields Equation (6).

We can also show Equation (6) without introducing the configuration-space field [thus,  $g(\mathbf{x}) = 1$  below]. Instead, we now assume that each trajectory frame  $\mathbf{x}$  is free to choose the state according to the Bayes' rule [70,71]: since the prior probability of state  $i$  is  $N_i / N_{\text{tot}}$ , and the conditional probability of observing  $\mathbf{x}$  in state  $i$  is  $w_i(\mathbf{x}) \equiv q_i(\mathbf{x}) / Z_i$ , the posterior probability of  $\mathbf{x}$  being in state  $i$  is given by [11]

$$p(i|\mathbf{x}) = \frac{(N_i / N_{\text{tot}}) w_i(\mathbf{x})}{\sum_{k=1}^K (N_k / N_{\text{tot}}) w_k(\mathbf{x})}. \quad 110$$

Summing this over all trajectory frames  $\mathbf{x}$  (no matter the original state  $j$ ) yields the expected population of state  $i$ ,

$$\hat{N}_i = \sum_{\mathbf{x}} p(i|\mathbf{x}) = \sum_{\mathbf{x}} \frac{N_i w_i(\mathbf{x})}{\sum_{k=1}^K N_k w_k(\mathbf{x})}, \quad (\text{A3}) \quad 115$$

where  $\sum_{\mathbf{x}} \equiv \sum_{j=1}^K \sum_{\mathbf{x}}^{(j)}$ . If we demand  $\hat{N}_i$  to be equal to the  $N_i$ , Equation (6) is recovered. Alternatively, by following the argument used in the



expectation-maximisation algorithm, [11,71–74] we can view Equation (A3) as the result of maximising the probability of observing the trajectory  $\{\mathbf{x}\}$ ,

$$p(\{\mathbf{x}\}|N_1, \dots, N_K) \propto \prod_{k=1}^K \sum_{\mathbf{x}} (N_k/N_{tot}) w_k(\mathbf{x}),$$

with respect to variations of  $N_i$  under the constraint  $\sum_{i=1}^K N_i = N_{tot}$ .

## Appendix 2. Models for the convergence of direct WHAM

Here, we use simple models to study the convergence of direct WHAM. We shall show that slow convergence is associated to a wide temperature range, especially with a large spacing.

### Linearised WHAM equation

Consider  $K$  distributions,  $\rho_i(E)$ , at different temperatures,  $\beta_i$  ( $i = 1, \dots, K$ ), normalised as  $\int \rho_i(E) dE = 1$ . For simplicity, we assume equal sample sizes,  $N_i$ . Then, Equation (4), can be written in the iterative form as

$$f_i^{(new)} = -\log \int \frac{\sum_{k=1}^K \rho_k(E) \exp(-\beta_i E)}{\sum_{k=1}^K \exp(-\beta_k E + f_k^{(old)})} dE. \quad (B1)$$

Around the true solution,  $f^* = (f_1^*, \dots, f_K^*)$ , the equation can be linearised as

$$\delta f_i^{(new)} = \sum_{j=1}^K A_{ij} \delta f_j^{(old)},$$

where  $\delta f_i^{(new/old)} \equiv f_i^{(new/old)} - f_i^*$ , and

$$A_{ij} = \int \frac{\sum_{k=1}^K \rho_k(E) e^{-(\beta_i + \beta_j)E + f_i^* + f_j^*}}{D^2(E; f^*)} dE. \quad (B2)$$

With  $D(E; f^*) = \sum_{k=1}^K e^{-\beta_k E + f_k^*}$ . In matrix form, we have  $\delta f^{(new)} = A \delta f^{(old)}$ .

The elements of matrix  $A$  are positive, i.e.  $A_{ij} > 0$ , and normalised, i.e.

$$\sum_{i=1}^K A_{ij} = 1. \quad (B4)$$

The latter can be seen from Equation (B1) with  $f_i^{(new/old)} \rightarrow f_i^*$ . Besides,  $A$  is symmetric:

$$A_{ij} = A_{ji}. \quad (B4)$$

Thus,  $A$  can be regarded as a transition matrix. [4] Each left eigenvector  $\mathbf{c} = (c_1, \dots, c_K)$  of  $A$  is associated to a mode of  $\delta f$  and the eigenvalue  $\lambda$  gives the rate of error reduction during iteration. That is,  $\sum_{i=1}^K c_i \delta f_i$  decays as  $\lambda^n$  asymptotically with the number of iterations,  $n$ .

The largest eigenvalue is  $\lambda_0 = 1.0$ , and its eigenvector  $\mathbf{c} = (1, \dots, 1)$  corresponds to a uniform shift of all  $\delta f_i$ , which is unaffected by the iteration, i.e.  $\sum_{i=1}^K \delta f_i^{(new)} = \sum_{i=1}^K \delta f_i^{(old)}$ , as a consequence of Equation (B3). The next largest eigenvalue,  $\lambda_1$ , determines the rate of convergence of the slowest mode, and a larger value of  $1 - \lambda_1$  means faster convergence. Below, we determine  $\lambda_1$  in a few solvable cases.

### Exact distribution approximation (EDA)

To proceed, we assume that the observed distributions are exact, and thus the solution,  $(f_1^*, \dots, f_K^*)$ , is also exact. Then, for any  $k$ , we have

$$\rho_k(E) = g(E) e^{-\beta_k E + f_k^*}, \quad (B5)$$

with  $g(E)$  being the density of states. This simplifies Equation (B2) as

$$A_{ij} = \int \frac{g(E) e^{-(\beta_i + \beta_j)E + f_i^* + f_j^*}}{D(E; f^*)} dE. \quad (B6)$$

### Gaussian density of states

Further, we approximate  $g(E)$  as a Gaussian. [14] With a proper choice of the multiplicative constant of  $g(E)$ , we have,

$$g(E) = \sqrt{\frac{a}{2\pi}} \exp\left[-\frac{1}{2}a(E - E_c)^2\right]. \quad (B7)$$

It follows

$$f_i = -\log \int g(E) \exp(-\beta_i E) dE = \beta_i E_c - \frac{\beta_i^2}{2a}, \quad (B8)$$

and

$$\rho_i = \sqrt{\frac{a}{2\pi}} \exp\left[-\frac{1}{2}a\left(E - E_c + \frac{\beta_i}{a}\right)^2\right].$$

Thus, the distribution at any temperature is a Gaussian of the same width  $\sigma_E = 1/\sqrt{a}$ . The inverse temperature  $\beta_i$  affects the energy distributions only as a linear shift to the distribution centre. It follows that both the origin of  $\beta$  and that of  $E$ , represented by  $E_c$ , can be set to any values that help calculation, without affecting the value of  $A_{ij}$ .

### Two-temperature case

For the two-temperature case, the matrix  $A$  has only one free variable because of Equations (B3) and (B4), and it can be written as

$$A = \begin{pmatrix} 1 - A_{12} & A_{12} \\ A_{12} & 1 - A_{12} \end{pmatrix}. \quad (B9)$$

Thus, the second largest eigenvalue is  $\lambda_1 = 1 - 2A_{12}$ .

Under EDA, we have, from Equations (B5) and (B6),

$$A_{12} = \int \frac{\rho_1(E) \rho_2(E)}{\rho_1(E) + \rho_2(E)} dE \leq \int \frac{\rho_1(E) + \rho_2(E)}{4} dE = \frac{1}{2}, \quad (B10)$$

where the equality is achieved only for identical distributions. Geometrically,  $A_{12}$  represents the degree of overlap of the distributions, as shown in Figure B1(a), and it decreases with the separation of the two distributions, from the maximal value,  $1/2$ , achieved at  $\beta_1 = \beta_2$ .

By further assuming a Gaussian density of states, we can, without loss of generality, set  $\beta_1 = -\sigma_\beta$ ,  $\beta_2 = \sigma_\beta$ , and  $E_c = 0$ . Then, from Equations (B6), (B7) and (B8), we have

$$1 - \lambda_1 = 2A_{12} = \sqrt{\frac{a}{2\pi}} \int \frac{\exp[-aE^2/2 - \sigma_\beta^2/(2a)]}{\cosh(\sigma_\beta E)} dE \approx \frac{e^{-\sigma_\beta^2 \sigma_E^2/2}}{\sqrt{1 + \sigma_\beta^2 \sigma_E^2}} \left[ 1 + \frac{\sigma_\beta^4 \sigma_E^4}{4(1 + \sigma_\beta^2 \sigma_E^2)^2} \right], \quad (B11)$$

where  $\sigma_E = 1/\sqrt{a}$ , and we have used  $1/\cosh x \approx \exp(-x^2/2)(1 + x^4/12)$ . This model shows a rapid decrease in the rate of convergence of direct WHAM with the temperature separation.

### Three-temperature case

Similarly, for three evenly spaced temperatures, we can, without loss of generality, set  $\beta_1 = -\Delta\beta$ ,  $\beta_2 = 0$ , and  $\beta_3 = \Delta\beta$ , with  $\Delta\beta = \sqrt{\frac{3}{2}}\sigma_\beta$ . Then,

$$1 - \lambda_1 = A_{12} + 2A_{13} \approx \mathcal{A}\left(\sqrt{\frac{3}{8}}\sigma_\beta\sigma_E, -\frac{5}{2}\right) + 2\mathcal{A}\left(\sqrt{\frac{3}{2}}\sigma_\beta\sigma_E, \frac{1}{2}\right), \quad (B12)$$

40

45

50

55

60

65

70

75

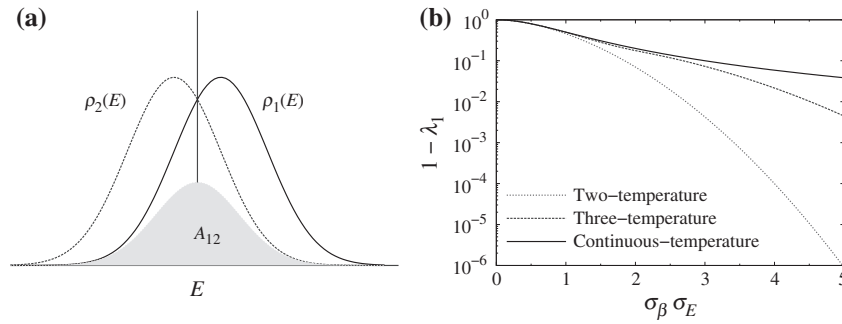


**Figure B1.** (a)  $A_{12}$ , which determines the rate of convergence in the two-temperature case, as a measure of overlap of the two energy distributions. (b) Comparison of the rates of convergence in the two-, three- and continuous-temperature cases, Equations (B9), (B10), and (B12), respectively. Here,  $\sigma_\beta$  is the standard deviation of the  $\beta$  distribution;  $\sigma_E$  is that of the energy distribution at any temperature. A larger value of  $1 - \lambda_1$  means faster convergence.

here

$$\mathcal{A}(b, t) = \frac{e^{-b^2/2} / (1 + \frac{1}{2} e^{tb^2})}{2 \sqrt{1 + b^2 / (1 + \frac{1}{2} e^{tb^2})}} \left[ 1 + \frac{(2 - \frac{1}{2} e^{tb^2}) b^4 / 8}{(1 + b^2 + \frac{1}{2} e^{tb^2})^2} \right].$$

### Continuous-temperature case

If there are a large number  $K$  of temperatures in a finite range, we can approximate them by a continuous distribution,  $w(\beta)$ . In this case, the sum over temperatures can be replaced by an integral:  $\sum_{k=1}^K \rightarrow K \int d\beta w(\beta)$ .

The eigenvalue  $\lambda_l$  and eigenvector  $c_l(\beta)$  are now determined from the integral equation

$$K \int w(\beta') c_l(\beta') A(\beta, \beta') d\beta' = \lambda_l c_l(\beta), \quad (\text{B11})$$

where  $A(\beta, \beta')$  is  $A_{ij}$  with  $\beta_i \rightarrow \beta$  and  $\beta_j \rightarrow \beta'$ .

Equation (B11) can be solved in a special case, in which we assume EDA, Equation (B6), a Gaussian density of states, Equation (B7), and a Gaussian  $\beta$  distribution:

$$w(\beta) = \frac{1}{\sqrt{2\pi} a'} \exp \left[ -\frac{(\beta - \beta_c)^2}{2 a'^2} \right],$$

with width  $\sigma_\beta = \sqrt{a'}$ . The physical solution is

$$\lambda_l = \left( \frac{a'}{a + a'} \right)^l, \\ c_l(\beta) = H_l \left( \frac{\beta - \beta_c}{\sqrt{2} a'} \right),$$

where  $H_l(x)$  is the Hermite polynomial, [49–51] generated as  $c_l(x) = \sum_{l=0}^{\infty} H_l(x) t^l / l!$ . Thus, for the second largest eigenvector, we have

$$1 - \lambda_1 = \frac{1}{1 + \sigma_\beta^2 \sigma_E^2}, \quad (\text{B12})$$

which decreases with increasing temperature range,  $\sigma_\beta$ , albeit more slowly than the two- and three-temperature values, as shown in Figure B1(b). Thus, Equation (B12) only gives an upper bound, and non-zero spacing between temperatures can further slow down the convergence. Besides, sampling error, which is ignored in the above calculation, may also slow down the convergence.